Determination of branch fraction and minimum dimension of mass-fractal aggregates

G. Beaucage*

Department of Chemical and Materials Engineering, University of Cincinnati, Cincinnati, Ohio 45221-0012, USA
(Received 23 March 2004; published 8 September 2004)

Particles of micrometer to nanometer size often aggregate to form branched structures. Such materials include metals and metal oxides as well as biological and polymeric materials (considering the persistence length as a primary unit). Characterization of such structures is difficult since they typically display disordered, irregular features in three dimensions. Branched aggregates display two limiting size scales: that of the primary particle, R_1 and that of the aggregate, R_2. The mass-fractal model is often used to describe such structures where the aggregate mass, $z = M_2/M_1$, is related to the aggregate size, $r = R_2/R_1$, through a scaling relationship $z = \alpha r^{d_f}$, where the lacunarity α is close to 1 and may depend on the growth mechanism. Scattering of x rays, light and neutrons yields a direct measure of the mass-fractal dimension since $I(q) \sim q^{-d_f}$ for $1/R_2 < q < 1/R_1$ using scaling arguments. For linear, monodisperse aggregates with convoluted chain paths, analytic functions describing both the scaling and larger-size aggregate scattering regimes have been reported. For example, the Debye function for linear, Gaussian coils describes scattering when $d_f = 2$. Real, mass-fractal aggregates, however, can display variability from the linear chain, monodisperse model. Often the branch content is of vital importance to understanding both the growth of aggregates and their physical properties, especially dynamic properties. An approach is presented for the analysis of aggregate branching from static small-angle scattering. Comparison is made with analytic, simulation, and experimental results from the literature.

I. INTRODUCTION

High-surface-area, particulate materials often aggregate into loosely branched structures due to a competition between the kinetic laws governing transport and bonding and the reduction in free energy associated with a reduction in surface area. In polymeric materials, directional bonding leads to molecular chain aggregates that can be topologically linear and in some ways structurally analogous to particulate aggregates. For ceramic aggregates formed by partial sintering [1] or partial Ostwald ripening [2,3] of nanoscale primary particles, such directional bonding is rare (governed by crystallographic features [4] when it occurs) and branched structures are more common. Similarly, pharmaceutical materials can display ramified aggregate structures [5]. Recently, branched aggregate structures have also proven important to models for glass formation [6]. The branch content of aggregate or polymeric structures is of vital importance to physical properties, especially when considering dynamics. The viscosity of polymer melts, for instance, is greatly affected by branch content [7]. Similarly, the reinforcement of elastomers by ceramic aggregates is governed by branch content [8,9]. For pharmaceutical systems it has recently been shown that bioactivity is strongly influenced by aggregation [5].

A. Aggregate scattering

Quantification of branch content is challenging since aggregates follow three-dimensional mass scaling [10] hindering two-dimensional (2D) imaging techniques [11–14] especially when $d_f > 2$ [12]. Even when microscopy has been used to quantify branching, [6,11–19] the approach has proven tedious and the results generally qualitative. A simple, direct measure of the branch content for aggregates is highly desirable both for modeling of growth as well as for understanding the properties of mass-fractal aggregates, especially dynamic properties.

Static-scattering techniques have been used to great success in characterizing disordered aggregate structures [10,11,13,14,20–22]. Generally, Guinier's law [23]

$$I(q) = G \exp\left(\frac{-(qR_g)^2}{3}\right) \tag{1}$$

and the fractal scaling law [11]

$$I(q) = B_f q^{-d_f} \tag{2}$$

have been found useful to locally describe the signature of mass-fractal aggregates in scattering, where $q = (4\pi/\lambda)\sin(\theta/2)$ and θ is the scattering angle, R_g is the radius of gyration for the aggregate, G is defined as $N n_e^2$ where N is the number density of particles and n_e is the number of electrons (for x-ray scattering) in a particle, d_f is the mass-fractal dimension, and B_f is the scaling prefactor in the fractal, power-law regime [22]. The primary particle contribution to scattering occurs at smaller sizes and is indicated by a second, high-q Guinier function G_1, $R_{g,1}$, as well as, often, a scaling regime reflecting Porod's law [24]:

$$I(q) = B_P q^{-4}, \tag{3}$$

where $B_P = 2\pi G_1 S_1 / V_1^2$, and S_1 and V_1 are the surface area and volume of the primary particles. The index 1 refers to the smallest-size scale for the aggregate, the primary particle.

*Currently on sabbatical leave at Institut für Verfahrenstechnik, ETH Zentrum, ML F 26 CH-8092 Zürich, Switzerland.

These local, scattering laws describe the overall structural size, Eq. (1), and mass/surface scaling (2) and (3) of a structure. The local laws cannot independently describe topological features such as branch content. For example, a Gaussian linear chain displays $d_f=2$ and follows Eq. (2) in the same way that a randomly oriented disk displays the scaling signature of a two-dimensional structure. The two structures cannot be distinguished by the power-law scaling regime alone. Similarly, the Guinier regime cannot independently distinguish between disk and linear Gaussian scattering. This is a manifestation of the loss of phase information inherent to static scattering. However, the power-law and Guinier regimes of scattering reflect different average attributes of a fractal structure and in combination can yield new information. By describing the scattering curve across multiple regimes, information pertaining to topology can be ascertained from a static measurement as is supported by the difference between scattering functions for two-dimensional objects of different topology—e.g., disks and Gaussian coils, described later.

A global scattering function [22,25–27] for mass-fractal aggregates has been previously reported and demonstrated. For aggregates with primary particles that display sharp smooth interfaces, scattering can be represented by seven parameters, with index "1" representing the primary particles and index "2" the aggregates G_1, $R_{g,1}$, B_P and G_2, $R_{g,2}$, B_f, d_f. From the three parameters associated with the primary particles we can calculate the primary-particle size d_p as the ratio of the third to the second moment of size, the polydispersity of primary particles, and the number density of primary particles [28,29].

By combination of the primary and aggregate parameters, the degree of aggregation, z, can be calculated in several ways [22,28]. z reflects the number of primary particles in an aggregate and is proportional to the aggregate mass. Using the Guinier prefactors of Eq. (1), the ratio of the second and first moments of the number distribution of z is obtained [22,28]:

$$z_{2:1} = \frac{G_2}{G_1} = \frac{\langle z^2 \rangle}{\langle z \rangle}, \qquad (4)$$

since $G_2 = N_2 n_{e,2}^2 = N_2 z^2 n_{e,1}^2$ and $G_1 = N_1 n_{e,1}^2 = N_2 z n_{e,1}^2$, where N_2 is the number density of aggregates, $n_{e,2}$ is the average number of electrons in an aggregate, N_1 is the number density of primary particles, and $n_{e,1}$ is the number of electrons in a primary particle. The superscript on z in Eq. (4) is associated with the source moments. This calculation involves no assumptions concerning the aggregate structure except that the particles described by G_1 aggregate to form the structure described by G_2. z can also be calculated using structural sizes and scaling from scattering [30].

Chainlike aggregates, which do not display branching, are termed "linear" aggregates. For instance, a linear polymer chain in a θ solvent, a random walk, displays a dimension $d_f = 2$ [31], while a *linear* chain in a good solvent, self-avoiding walk, displays a dimension $d_f = 5/3$ [31–33]. For monodisperse, linear aggregates the parameter B_f of Eq. (2) is uniquely related to the other aggregate scattering parameters [22,25,27]:
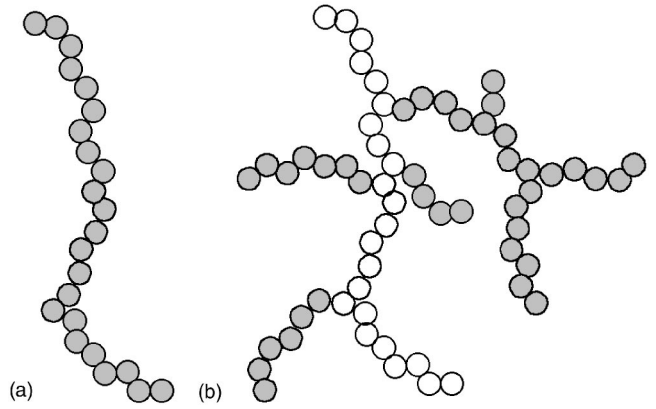
FIG. 1. 2D schematic sketches of aggregates with similar R_g. (a) Linear aggregate and (b) a branched fractal aggregate of identical p but different z and d_f, as described in the text.

$$B_{f,c=1} = \frac{G_2 d_f}{R_{g,2}^{d_f}} \Gamma\left(\frac{d_f}{2}\right), \qquad (5)$$

where $\Gamma()$ is the gamma function. For branched aggregates, Eq. (5) is no longer appropriate since it is based on an asymptotic value from an integral for linear structures [22,34]. Equation (5) will be modified to account for branched structures in this article. First, scaling laws for branched aggregates will be summarized.

B. Scaling laws for branched aggregates

In Fig. 1, a linear chain aggregate and a branched aggregate are schematically represented in two dimensions. The branched aggregate, Fig. 1(b), can be described in terms of a minimum path across the aggregate, open circles in Fig. 1(b), which is, in this case, identical to the linear chain path of Fig. 1(a). It is convenient to describe a scaling relationship between the number of primary particles in this minimum path, p [open circles Fig. 1(b)], with the aggregate size R_2 and with the degree of aggregation, z [8,35]:

$$p^c \sim z \sim \left(\frac{R_2}{R_1}\right)^{d_f}, \qquad (6)$$

where c is the connectivity dimension and R_1 is the size of the primary particles or the smallest size displayed by the aggregate. (c is also termed the intrinsic dimension [36].) The minimum path is a fundamental feature of a branched aggregate and describes the scaling behavior of branching with mass in terms of c and z. Since Eq. (6) relies on z, it is inherently necessary to know the structure of the primary particle, R_1, to determine features related to aggregate branching, the second scaling relationship of Eq. (6). c is 1 for a linear chain and increases to d_f with increased aggregate branching. A "regular object"—for example, a rod, disk, or sphere—is defined by $c=d_f$.

Furthermore, it is convenient to describe a direct scaling relationship for p with the aggregate size, R_2/R_1 [8,35]:

TABLE I. Values of d_f, c, d_{min}, and B_f for several well-described structures.

	Disk [23]	Rod [23]	Gaussian [31,38] (random walk)	Good solvent [31–33] (self-avoiding walk)
d_f	2	1	2	5/3
c	2	1	1	1
d_{min}	1	1	2	5/3
Object Type	regular	regular and fractal	fractal	fractal
B_f Analytic	G_2/R_g^2	$\pi G_2/(\sqrt{3}R_g)=1.81\ G_2/R_g$	$2G_2/R_g^2$	unknown
B_f Eq. (5′)	G_2/R_g^2	$1.77\ G_2/R_g$	$2G_2/R_g^2$	$5\Gamma(5/6)G_2/(3R_g^{5/3})$

$$p = \left(\frac{R_2}{R_1}\right)^{d_{min}}, \qquad (7)$$

where d_{min} is called the minimum dimension. d_{min} is 1 when a linear path from one side to the other of an aggregate can be made through the structure—i.e., for "regular objects." For linear chains, $c=1$ and $d_{min}=d_f$. d_{min} drops with increased branching. From Eqs. (6) and (7) a relationship between c, d_{min}, and d_f is available,

$$c = \frac{d_f}{d_{min}}, \qquad (8)$$

so that only two principle scaling dimensions are needed to describe a branched aggregate. d_f in Fig. 1(a) is identical to d_{min} in Fig. 1(b) so that the branched aggregate might be described as z/p superimposed chains of dimension d_{min}.

Table I gives values for well-described regular ($d_f=c$) and mass-fractal structures to clarify the use of Eqs. (6)–(8). A regular structure is considered, in this context, as a fully branched object of mass-fractal dimension d_f. In addition to these scaling relationships, a regular object displays the highest degree of asymmetry possible for a given value of d_f.

The number fraction of branches, ϕ_{br}, in an aggregate can be calculated from

$$\phi_{br} = \frac{z-p}{z} = 1 - z^{1/c-1} = 1 - \left(\frac{R_{g,2}}{R_{g,1}}\right)^{d_{min}-d_f}. \qquad (9)$$

However, the number of branches in an aggregate, n_{br}, can only be calculated if the mass of an average branch, z_{br}, is known,

$$n_{br} = \phi_{br}\frac{z}{z_{br}}, \qquad (10)$$

where z_{br} is the number of primary particles in an average branch. The situation can become fairly complicated if multiple generations of branching occur in a hierarchical structure such as an arborial or dendric polymer [37]. Nonetheless, the branch fraction, Eq. (9), remains a viable measure of branch content on a relative and absolute scale. Figure 2 shows the behavior of ϕ_{br} for branched aggregates of variable z as a function of c. The branch fraction is of limited sensitivity for large c or large z, Eq. (9). The connectivity dimension c varies from 1 for a linear chain to d_f for a regular object. For a series of aggregates with variable connectivity dimension c but with a fixed number of primary particles, z, the branch content increases in a nonlinear fashion with c as shown in Fig. 2. Figure 2 is intended to indicate the optimal range of sensitivity for the branch fraction—i.e., small c and relatively small z.

At times it is useful to describe the average coordination number c_N for primary particles in a branched aggregate [1]:

$$c_N = 2 + \frac{n_{br}}{z} = 2 + \left(\frac{\phi_{br}}{z_{br}}\right). \qquad (11)$$

The coordination number also depends on the mass of an average branch, z_{br}.

C. Disk versus Gaussian, linear-chain scattering

For a monodisperse population of aggregates, Eq. (5) is not correct if the aggregates are nonlinear. For instance, for objects with $d_f=2$, the extremes of a Gaussian, linear polymer and a disk can be considered, Table I. The scattering function for a disk of radius R [23] ($2R_g^2=R^2$),

$$I(q) = \frac{2G_2}{R^2}q^{-2}\left[1 - \frac{J_1(2qR)}{qR}\right]$$

$$= \frac{G_2}{(qR_g)^2}\left[1 - \frac{J_1(2(2^{1/2})qR_g)}{2^{1/2}qR_g}\right] \text{disk}, \qquad (12)$$

indicates $B_f=G_2/R_g^2$, from the scaling prefactor in Eq. (12), whereas Eq. (5) yields the value for a Gaussian, linear-chain aggregate, $B_f=2G_2/R_g^2$ as can also be obtained from the De-
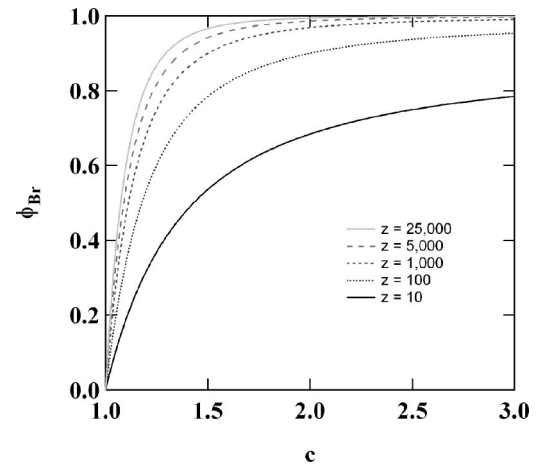
FIG. 2. Dependence of branch fraction, Eq. (7), on connectivity dimension c and number of primary particles in an aggregate, z.
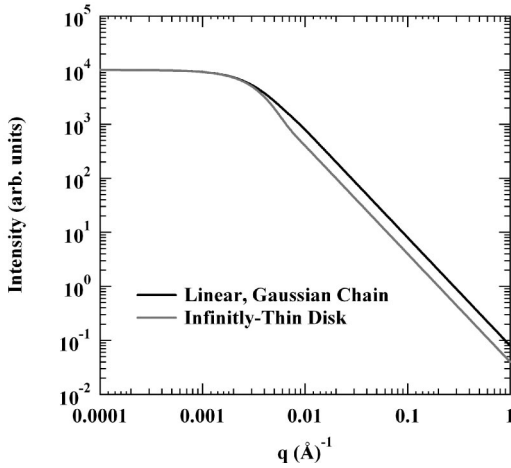
FIG. 3. Log scattered intensity versus log q for monodisperse, linear-Gaussian chains, and a scaling function for disk scattering in the aggregate regime using the unified function [22,23,25,26,38].

bye scattering function for a monodisperse, linear chain in extrapolation [22,34,38]:

$$\frac{I(q)}{G} = \frac{2\{(qR_g)^2 - 1 + \exp[-(qR_g)^2]\}}{(qR_g)^4} \quad \text{linear, Gaussian.}$$

$$(13)$$

Then, from the extremes of linearity and branching in 2D-objects, the power-law prefactor B_f decreases with branch content relative to G_2 and $R_{g,2}$. This means that the scattering curve for branched structures will display a weak knee in the mass-fractal regime for a log-log plot, as shown in Fig. 3, $q=0.003$ for the disk, scaling function. Such a weak knee was also noted by Thouy and Jullien for branched aggregates [39]. It should be noted that a monodisperse disk displays oscillations in the scattering pattern, as indicated by Eq. (12), which are not shown in the scaling function of Fig. 3. The knee feature could be overlooked in the absence of a comparable linear scattering function. Even the most extreme case for $d_f=2$, Fig. 3, shows only a weak deviation from the linear curve. The knee is expected to be more prominent for higher d_f since d_f and branching are related as discussed below.

From such comparisons it is expected that information concerning the branch content of aggregates might be available from static-scattering measurements if a direct comparison between the Guinier and power-law scaling regimes of aggregate scattering is made and if a sufficient range of q is observed.

D. Mass-fractal correlation function

A scaling form for mass-fractal scattering in the power-law regime, Eq. (2), is calculated using the pairwise correlation function [10,11,14,21],

$$\gamma(r) \sim r^{d_f - 3} \quad \text{for } R_1 \leqslant r \leqslant R_2, \qquad (14)$$

where r is a correlation distance associated with the scattering measurement, $r \sim 1/q$. For $r < R_1$, $\gamma(r) = 1$, and for

$r > R_2$, $\gamma(r) = 0$. The scattered intensity at q is given by the Fourier transform of $\gamma(r)$ for spherically symmetric objects (on average) [11]:

$$I(q) \sim \frac{z^2}{R_2^3} \int_0^\infty r\gamma(r) \frac{\sin(qr)}{q} dr \sim \frac{z^2}{(qR_2)^{d_f}} \int_0^{qR_2} y^{d_f - 2} \sin(y) dy,$$

$$(15)$$

where the last scaling relationship in Eq. (15) substitutes $y = qr$ and where $\gamma(r)$ reaches 0 at the finite size of the aggregate, R_2, making the last integral always finite, even when $d_f \geqslant 2$ [11]. Additionally, it is assumed that the last integral is independent of q in the fractal scaling regime.

Various *ad hoc* "cutoff" functions $h(r/\xi)$ have been proposed for Eq. (14) to account for the decay in correlation at the aggregate size, R_2 [10,11,21]:

$$\gamma(r) \sim h\left(\frac{r}{\xi}\right) r^{d_f - 3}, \qquad (14')$$

with the most common being an exponential decay as originally proposed by Jullien [11]. An alternative to consideration of scaling functions, Eqs. (14) and (14′), is to modify the exact calculation of Debye for a linear, Gaussian chain [38] that results in Eq. (13), as first proposed by Benoit [34]. The Debye-Benoit approach is used to obtain Eq. (5) in extrapolation, for instance [22].

II. SCATTERING FUNCTION FOR BRANCHED AGGREGATES

A. Modification of the Benoit function for branched aggregates

Benoit [34] introduced an integral function for scattering from linear chain aggregates of arbitrary mass-fractal dimension d_f,

$$\frac{I(q)}{G} = \frac{d_f}{(qR_g)^{d_f}} \int_0^{(qR_g)^2} \left[1 - \frac{y^{d_f/2}}{(qR_g)^{d_f}}\right] e^{-y} y^{((d_f/2)-1)} dy,$$

$$(16)$$

which is obtained from Debye and Peterlin's integral form [38,40]

$$\frac{I(q)}{G} = \frac{2}{z^2} \int_0^z (z - n) e^{-q^2 R_{g,n}^2} dn, \qquad (16')$$

with the substitution of

$$y = q^2 R_{g,n}^2, \qquad (17)$$

$$n = \left(\frac{6R_{g,n}^2}{R_1^2}\right)^{d_f/2} = \left(\frac{6y}{q^2 R_1^2}\right)^{d_f/2}, \qquad (18)$$

and

$$z = \left(\frac{6R_g^2}{R_1^2}\right)^{d_f/2}, \qquad (19)$$

where R_g is the aggregate radius of gyration and $R_{g,n}$ is the radius of gyration of a linear aggregate of length n. The term

"6" in the description of n and z assumes Gaussian scaling and can more correctly be written $(d_f/2+1)(d_f/2+2)$ when d_f deviates from 2 [22]. However, this term cancels in Eq. (16), so the exact value is of limited consequence. In Eq. (16'), n is the local chain index which progresses from 0 to z, and z is the overall linear-chain length. The lead term in Eq. (16) includes d_f which arises from the substitution of dy for dn in Eq. (16') using

$$dn = \frac{d_f(6)^{d_f/2}}{2R_1^{d_f}q^{d_f}}y^{(d_f/2)-1}dy. \tag{20}$$

Extrapolation to high q of the integral in Eq. (16) leads to Eq. (5) as shown by Benoit. Use of $d_f=2$ in Eq. (16) leads directly to Eq. (13). If d_f deviates from 2, Eq. (16) can not be analytically solved as noted by Benoit [34].

The Benoit integral, Eq. (16), is interesting in that it contains a kind of "cutoff" function since the bracketed term and exponential term go to 0 near the aggregate size [10,11,21]. This cutoff function is natural to the linear-chain integral and is not an *ad hoc* function such as the exponential functions previously used in the literature [21].

Equations (16) and (16') are useful for linear chains where the chain index linearly follows n and it is within this context that both the Debye function for polymer coils, Eq. (13), [38] and Benoit's function, Eq. (16), were obtained. For branched chains, the integral in y, Eq. (16), cannot progress linearly for the z primary particles of the aggregate since such a linear indexing scheme is not unique for a branched aggregate.

Debye's derivation of the polymer chain function, Eq. (16'), ignores correlations between chain segments that are not topologically connected [38]. Following a similar assumption, a branched aggregate can be considered, Fig. 1(b), as being composed of a collection of (z/p) minimum paths. Then Eq. (16') is written, for a branched aggregate,

$$\frac{I(q)}{G} = \left(\frac{2}{p^2}\right)p^{1-c}\int_0^p n^{c-1}(p-n)e^{-q^2R_{g,n}^2}dn, \tag{21}$$

where p^{1-c} normalizes for the number of minimum paths in the aggregate, $z/p = p^{c-1}$. n^{c-1} accounts, within the integral, for the average number of minimum paths with a path length n. Equation (21) ignores correlations between branches just as Eq. (16) ignores correlations between chain segments that are not linearly bonded. The integral is over the minimum path and follows a unique, average minimum path index, n goes from 0 to p. Substitution is made, following Debye and Benoit, except that all terms are defined for the minimum path using the minimum dimension,

$$n = \left(\frac{6R_{g,n}^2}{R_1^2}\right)^{d_{min}/2} = \frac{1}{q^{d_{min}}}\left(\frac{6y}{R_1^2}\right)^{d_{min}/2} \tag{22}$$

and

$$z = \left(\frac{6R_g^2}{R_1^2}\right)^{d_{min}/2}, \tag{23}$$

parallel to Eqs. (18) and (19). With these substitutions a modified form of Eq. (16) is obtained:

$$\frac{I(q)}{G} = \frac{d_{min}}{(qR_g)^{d_f}}\int_0^{(qR_g)^2}\left[1 - \frac{y^{d_{min}/2}}{(qR_g)^{d_{min}}}\right]e^{-y}y^{((d_f/2)-1)}dy. \tag{24}$$

B_f for branched or linear aggregates arises from an extrapolation of Eq. (24) at high q as described by Benoit for Eq. (16) [34]:

$$B_f = \frac{G_2 d_{min}}{R_{g2}^{d_f}}\Gamma\left(\frac{d_f}{2}\right). \tag{5'}$$

Equation (5') allows for a direct determination of the branch fraction from the static scattering pattern of a monodisperse aggregate. [Equation (24) also contains a slightly modified "cutoff" function that includes the effect of branching through d_{min}.]

Equation (5') can be rearranged to calculate d_{min} from parameters measured directly in the static scattering pattern:

$$d_{min} = \frac{d_f}{c} = \frac{B_f R_g^{d_f}}{\Gamma(d_f/2)G}. \tag{25}$$

Equation (25) bears resemblance to the polydispersity parameter previously reported for solid particles [28]. Equation (5') agrees with analytic functions for regular and linear objects, correctly predicting the scaling prefactor for linear Gaussian coils, randomly oriented disks, and approximating the scaling prefactor for randomly oriented rods, Table I.

B. Polydisperse aggregates

Equations (5') and (25) give some indication of the consequences of polydispersity in aggregate size on the scattering curve. For linear aggregates, $c=1$, d_{min} should be equal to d_f, Eq. (25). However, the calculated d_{min} from Eq. (25) relies on the ratio of moments of z following Eqs. (4) and (4'') in [30]. The numerator in Eq. (25) reflects a higher-order moment, from the term R_g^{df} and Eq. (4'') [30], compared to the denominator, from the term G and Eq. (4). Then it is expected that for polydisperse, linear chains, d_{min} calculated using Eq. (25) will be larger than $d_{f,slope}$ observed as the negative of the slope of the power-law decay in the scattering pattern. An aggregate polydispersity index A can be considered to quantify this effect:

$$A = \frac{B_f R_g^{d_f}}{d_f\Gamma(d_f/2)G} = \frac{1}{c}, \tag{26}$$

where $-d_f$ is the observed power-law slope from the scattering pattern. Table II shows some possible values for A.

The last entry in Table II indicates that if no assumptions concerning aggregate size distribution or linearity are made, then analysis of static scattering data is limited. Generally, an assumption of either low aggregate polydispersity or low branch content will be necessary in analysis of static scattering from aggregates since, for the case of branched, polydisperse aggregates it is not possible to isolate the effects of dispersion and branching. (A description might be possible if sufficient TEM data on aggregate branching were available or if a model for aggregate growth predicted the branch con-

TABLE II. Aggregate polydispersity index A from Eq. (26) for several conditions.

	c	A
Linear, monodisperse	1	1
Linear, polydisperse	1	>1
Branched, monodisperse	>1	<1 (d_{min}/d_f)
Branched, polydisperse	>1	—

tent for instance. For branched polymers, separate measurement of the chain size distribution could be used or an assumption concerning the minimum dimension could be made.) In terms of B_f, branching and polydispersity have opposite consequences for the scattering curve, polydispersity serving to increase the power-law prefactor B_f relative to G and R_g and branching serving to decrease B_f, Fig. 3. In this article a narrow distribution in aggregate size is assumed and select systems of rather narrow aggregate size distribution are selected for comparison.

III. EVALUATION OF Eqs. (5′) AND (25) FOR BRANCHED AGGREGATES

A number of examples of branched aggregate and polymer scattering measurements and simulations exist in the literature for example, [10,11,21,37,39,41–44]. However, since Eqs. (5′) and (25) were derived for monodisperse aggregate size and because both the Guinier and mass-fractal scaling regimes must be observed, the number of viable systems for comparison is somewhat limited. Three examples will be shown: a randomly branched polymer in a good solvent [41], a recent study of diffusion-limited aggregation where changes in branch content and mass-fractal dimension with aggregate size can be considered [42], and a simulation by Hamsey and Jullien where diffusion-limited, ballistic and reaction-limited branched aggregates were considered [43]. In all three cases, scattering functions over a wide range of q have been reported. The literature scattering curves have been digitized and refit using the unified function [22,25–29] following the approach described in this article.

A. Antonitti DVB microgels

Antonietti and Rosenauer performed a careful neutron-scattering study of branched polystyrene in a good solvent (deuterated toluene) [41]. Figure 4 shows scanned data from Antonietti and the unified fits to the scanned data. The branched polystyrene was composed of 10% divinyl benzene (DVB) which acts as a random tetrafunctional branching agent with similar molecular weight to the monomer. The neutron scattering measurements were performed on 1% d-toluene solutions. Although radical polymerization was used, fairly narrow aggregate (chain) mass distribution were obtained by fractionation. The polydispersity index M_w/M_n is reported between 1.8 and 3 which is a narrow aggregate size distribution for branched polymers (M_w is the weight average molecular weight and M_n is the number average). The molecular weight, by light scattering, and the z values as
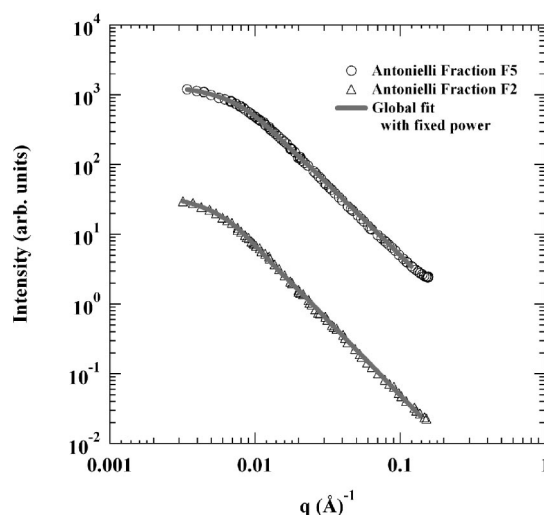
FIG. 4. Small-angle neutron scattering data from dilute solutions of branched polystyrene samples in deuterated toluene (scanned data from [41]). Two fractions are shown: F5 with $d_f=2.05$, $M_w=2\times10^6$ g/mol and F2 with $d_f=2.15$, $M_w=18\times10^6$ g/mol.

well as the fit and calculated values are reported in Table III for two fractions differing in molecular weight and branch content.

Using Eq. (25), the minimum dimension can be calculated from the global fits shown in Fig. 4 [22,25–29]. As noted in Table I, a linear polymer chain in a good solvent displays a self-avoiding walk with $d_f=5/3$ [31–33]. For good-solvent conditions it is expected that a lightly branched chain will display good-solvent scaling for the minimum path since the minimum path for the branched chain has some thermodynamic equivalence to the linear chain under these conditions; see schematic in Fig. 1. The value obtained for minimum dimension from the Antonietti data, Table III, matches the expected value of $5/3$ ($d_{min}\sim1.67$) for good-solvent scaling of a linear chain. The analysis indicates that the higher molecular weight fractions display a higher mass-fractal dimension due to higher branch content as indicated by the reduction in linearity, higher c, in Table I. The agreement between

TABLE III. Analysis of Antonietti and Rosenauer's branched polystyrene [41]. Two fractions were analyzed for d_{min} and branch fraction from small-angle neutron-scattering data. The values with reported error were free parameters in the unified fits of Fig. 4.

	F5	F2
M_w (g/mol)	2×10^6	18×10^6
G (arb. units)	1376 ± 8	38 ± 1
R_g (Å)	197 ± 1	268 ± 10
B_f	0.0448 ± 0.0004	0.00035
d_f	2.05	2.15
d_{min}	1.67	1.64
c	1.23	1.36
z	19 200	173 000
ϕ_{br}	0.84	0.94
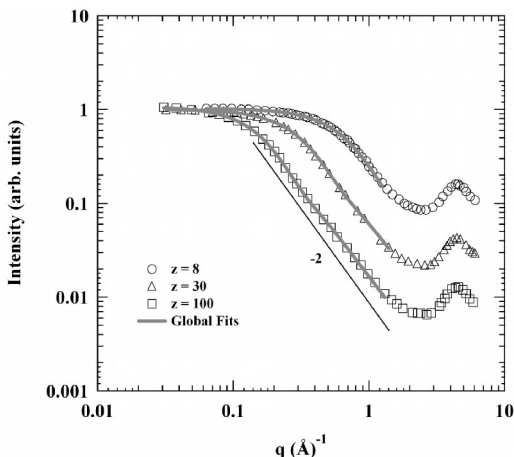
FIG. 5. Simulation results from Lattuada *et al.* [42] and global fits [22,25–29]. Simulations are for monodisperse aggregates formed by diffusion-limited aggregation. Table IV lists fit results and calculations. Line of slope −2 indicates Gaussian scaling for comparison.

the observed and expected d_{min} supports the validity of Eq. (25). The branch fraction is also reported in Table III using Eq. (9). Since the mean branch length is not known, the number of branches can not be calculated, Eq. (10).

B. Comparison with simulation results for monodisperse diffusion-limited aggregates (DLA)

Lattuada, Wu, and Morbidelli [42] report on simulation and experimental results for diffusion limited cluster-cluster aggregation. The simulation results are for monodisperse branched aggregates. Branch content was indirectly controlled through a sticking probability. The simulations were used to calculate the pairwise correlation function which was transformed into scattering functions for comparison with light-scattering data from colloidal aggregates. Scattering curves from simulations were reported as a function of z for small-z, monodisperse aggregates. Lattuada *et al.* also simulated scattering curves for large-z, polydisperse aggregates as a function of time of growth for comparison with experimental results.

Figure 5 shows simulated scattering data for the z comparison as well as fits using the unified function [22,25–29]. The fit results and calculations based on Eqs. (25) and (9) are shown in Table IV (first three data columns). The branch content, bottom row, is shown to increase monotonically with aggregate size z, following Eq. (9). The minimum path dimension remains constant within the resolution of the fit and an increase in the fractal dimension is related to a higher connectivity dimension—that is, more branches—for the larger aggregates. This is similar to the experimental study of Antonietti mentioned above except that the minimum dimension is not determined by thermodynamics in this case and has a lower value, 1.16 rather than 5/3. The minimum dimension in this case is apparently governed by the trajectory and sticking probability of the primary particles. These conditions remain constant for variable z leading to a constant d_{min}.

Lattuada *et al.* [42] also simulated growth by considering a time sequence growth for diffusion limited aggregation, Fig. 6(a), for polydisperse aggregates of large z. In analyzing the time-sequence data, low-polydispersity aggregates are assumed here, out of necessity. The fits to the simulations of Lattuada *et al.* show a decay in the minimum dimension towards 1 as growth proceeds, Fig. 6(b) and Table IV the last four columns, indicating a rapid increase in the connectivity of the aggregates as c approaches d_f. By 965 s the aggregates are close to "regular" objects. d_f is fairly constant but decreases slightly across the time series. This indicates that as the aggregates grow they become more branched but also display minimum paths with a lower degree of convolution; i.e., d_{min} drops. The reduction in convolution has a larger effect on d_f than the increased branching leading to a drop in d_f since $d_f = c \, d_{min}$. For these high-z aggregates the branch fraction rapidly approaches 1. The approach of d_{min} to 1 and c to d_f for diffusion-limited aggregates agrees with the simulations of Meakin *et al.* [36].

C. Comparison with simulation results for DLA, RLA, and ballistic growth

Table V shows results from fits to scanned, simulated scattered intensity from diffusion-limited, reaction-limited, and ballistic aggregates by Hasmy and Jullien [43]. An expected increase in d_f is seen across these three growth mechanisms. From unified fits using the approach outlined in

TABLE IV. Fit results and calculations from simulations by Lattuada *et al.* [42] of variable z and time for diffusion-limited aggregates. L8, L30, and L100 refer to Fig. 5 while the time series refer to Fig. 6.

	L8	L30	L100	125 s	275 s	515 s	965 s
G	1.03	1.01	1.08	1.24	15.4	150	1670
R_g	2.37	4.96	9.91	16800	23400	32900	45100
B_f	0.251	0.0617	0.0166	2.73×10^{-8}	2.06×10^{-7}	1.08×10^{-6}	7.73×10^{-6}
d_f	1.86	1.86	1.898	1.85	1.82	1.83	1.8
d_{min}	1.16	1.15	1.16	1.38	1.13	1.28	1.03
c	1.6	1.62	1.64	1.34	1.61	1.43	1.74
z	8	30	100	2069	3342	6518	9958
ϕ_{br}	0.54	0.73	0.83	0.95	0.99	0.98	1.00

(a)

(b)
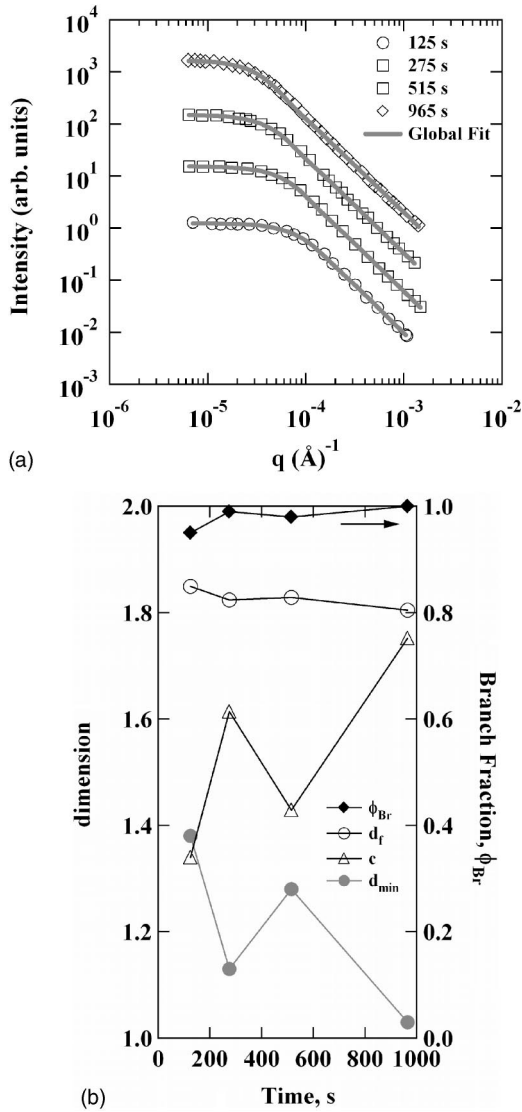
FIG. 6. (a) Lattuada time series simulation results (scattering data agree with experimental results in Ref. [42]). The simulations are for diffusion-limited aggregation with polydisperse aggregates. (b) Branch fraction, c, d_f, and d_{min} versus time from unified fits shown in (a).

this article, d_{min} increases in the order diffusion-limited aggregation (DLA), ballistic, reaction-limited aggregation (RLA), indicating that the minimum path is more convoluted for ballastic and reaction-limited growth compared to diffusion-limited growth. The connectivity dimension in-

TABLE V. Fit results from simulated scattering patterns of Hasmy and Jullien [43]. DL=diffusion-limited growth and RL=reaction limited growth. (The fit to the simulated scattering from diffusion-limited growth was for the low-q data only.)

	z	G	R_g	B_f	d_f	d_{min}	c	ϕ_{br}
DL (low-q)	4096	4000	76.5	6.45	1.60	1.43	1.11	0.56
Ballistic	4096	4150	44.6	4.19	1.95	1.62	1.20	0.75
RL	4096	4070	35.0	3.58	2.12	1.71	1.24	0.80

creases in the same order, indicating slightly higher branching, as reflected in the branch fraction ϕ_{br} from Eq. (9). Surprisingly, the largest effect, and the dominant one in terms of the fractal dimension, $d_f = c \, d_{min}$, comes from increased convolution of the minimum path rather than increased branching.

IV. CONCLUSION

An approach to the determination of branch content in aggregates using static, small-angle scattering was described. The approach requires measurement of the power-law scaling and Guinier regimes for the aggregates across a wide range of scattering vector. The branch fraction can be obtained if the degree of aggregation, z, is known. The topological dimensions d_{min} and c can be obtained by an extension of the structure factor for linear-chain aggregates following assumptions similar to those used by Debye in derivation of the linear, Gaussian structure factor for polymer coils. c and d_{min} can be used to describe branching in randomly aggregated structures. Structure factors for regular objects such as randomly oriented disks and rods can be reproduced as can the structure factor for a Gaussian coil and self-avoiding walks.

The approach was compared with one experimental study and with three simulation studies from the literature. Values for d_{min} measured in this way agree with the expected value of 5/3 for branched polymers in a good solvent from the experimental results of Antonietti and Rosenauer [41]. The aggregate-size simulations of Lattuada *et al.* [42] for monodisperse aggregates mimicked the experimental results of Antonietti and Rosenauer in that the minimum dimension remained fairly constant as the branch content increased with z. Diffusion-limited aggregate growth simulations of Lattuada *et al.* on polydisperse aggregates [42] showed growth dominated by branching and a terminal d_{min} that agrees with literature values [36]. For a series of three simulations by Hasmy and Jullien [43] on diffusion-limited, ballistic, and reaction-limited aggregation, the dominant difference in these growth mechanisms appears to be changes in the convolution of the minimum path rather than branching, although branching also increases for comparable simulations.

The proposed analysis of small-angle scattering data clarifies ambiguities associated with differences in scattering curves for linear, $c=1$, branched and regular, $c=d_f$, objects. Although a reconstruction of branched structures cannot be achieved from static-scattering data alone, consistent with the loss of phase information inherent to scattering techniques, significant average features of scaling and branch content are, in fact, available from a single static measurement if a sufficient range of scattering vector is probed. The information concerning branch content is contained in a scaling dimension for topology, d_{min} or c, which can be used to calculate the fraction of a structure that is not contained in the minimum path, p. This fraction is termed the branch fraction ϕ_{br}. If independent information is available concerning the length of an average branch, then the average coordination number and the number of branches in an aggregate can be determined from ϕ_{br}.

The approach presented in this article is intended for aggregates of low size dispersion since it is not possible to universally isolate the effects of dispersion in size from aggregate branch content. An index parameter, A, is suggested that can be used to qualitatively determine if the aggregate-size dispersion is important in extreme cases—that is, when $A > 1$. Determination of the branch fraction should be made with some caution when a wide dispersion in aggregate size is anticipated. It is shown that the effect of size dispersion and branch content are opposite in terms of the value of the scaling prefactor B_f; branching results in a lower value for B_f relative to G and R_g while polydispersity leads to a larger B_f. This indicates an underestimation of branching for polydisperse branched aggregates. It was demonstrated that the approach might be qualitatively useful even in cases of weak polydispersity, Fig. 6, if attention is paid to the possible consequences of polydispersity.

[1] S. K. Friedlander, *Smoke, Dust, and Haze: Fundamentals of Aerosol Dynamics* (Oxford University Press, New York, 2000).

[2] T. Sugimoto, *Monodisperse Particles* (Elsevier, New York, 2001).

[3] C. Brinker and G. Scherer, *Sol-Gel Science: The Physics and Chemistry of Sol-Gel Processing* (Academic, San Diego, CA, 1989).

[4] A. Singhal, L. M. Toth, G. Beaucage, J. S. Lin, and J. Peterson, J. Colloid Interface Sci. **194**, 470 (1997).

[5] S. L. McGovern, E. Caselli, N. Grigorieff, and B. K. Shoichet, J. Med. Chem. **45**, 1712 (2002); S. L. McGovern, B. T. Helfand, B. Feng, and B. K. Shoichet, *ibid.* **46**, 4265 (2003); J. Seidler, S. L. McGovern, T. N. Domain, and B. K. Soichet, *ibid.* **46**, 4477 (2003).

[6] E. R. Weeks, V. Prasad, J. C. Crocker, A. C. Levitt, A. Schofield, and D. A. Weitz, Science **287**, 627 (2000).

[7] J. N. Goodier, Philos. Mag. **22**, 678 (1936); H. M. Smallwood, J. Appl. Phys. **15**, 758 (1944); E. J. Guth, *ibid.* **16**, 20 (1945); P. G. Degennes, C. R. Seances Acad. Sci., Ser. B **286**, 131 (1978).

[8] T. A. Witten, M. Rubinstein, and R. H. Colby, J. Phys. II **3**, 367 (1993).

[9] D. J. Kohls and G. Beaucage, Curr. Opin. Solid State Mater. Sci. **6**, 183 (2002).

[10] J. E. Martin and A. J. Hurd, J. Appl. Crystallogr. **20**, 61 (1987).

[11] R. J. Jullien, J. Phys. I **2**, 759 (1992).

[12] M. Tence, J. P. Chevalier, and R. Jullien, J. Phys. (Paris) **47**, 1989 (1986).

[13] R. Jullien and R. Botet, *Aggregation and Fractal Aggregates* (World Scientific, Singapore, 1987).

[14] J. Teixeira, *On Growth and Forms, Fractal and Non-Fractal Patterns in Physics*, edited by H. E. Stanley and N. Ostrowski (Martinus Nijhoff, Boston, 1986), p. 145.

[15] G. C. Bushell, Y. D. Yan, D. Woodfield, J. Raper, and R. Amal, Adv. Colloid Interface Sci. **95**, 1 (2002).

[16] S. Tang, J. M. Preece, C. M. McFarlane, and Z. Zhang, J. Colloid Interface Sci. **221**, 114 (2000).

[17] U. O. Koylu, Y. Xing, and D. E. Rosner, Langmuir **11**, 4848 (1995).

[18] J. Cai, N. Lu, and C. M. Sorensen, Langmuir **9**, 2861 (1993).

[19] A. D. Dinsmore, E. R. Weeks, V. Prasand, A. C. Levitt, and D. A. Weitz, Appl. Opt. **40**, 4152 (2001).

[20] S. K. Sinha, Physica D **38**, 310 (1989).

[21] C. M. Sorensen, and G. M. Wang, Phys. Rev. E **60**, 7143 (1999).

[22] G. Beaucage, J. Appl. Crystallogr. **29**, 134 (1996).

[23] A. Guinier and G. Fournet, *Small-Angle Scattering of X-rays* (Wiley, New York, 1955).

[24] G. Porod, in *Small-Angle Scattering of X-rays*, edited by O. Glatter and O. Kratky (Academic, New York, 1982), pp. 17–52.

[25] G. Beaucage, J. Appl. Crystallogr. **28**, 717 (1995).

[26] G. Beaucage and D. W. Schaefer, J. Non-Cryst. Solids **172**, 797 (1994).

[27] J. Hyeon-Lee, G. Beaucage, S. E. Pratsinis, and S. Vemury, Langmuir **14**, 5751 (1998).

[28] G. Beaucage, H. K. Kammler, and S. E. Pratsinis, J. Appl. Crystallogr. **34**, 523 (2004).

[29] H. K. Kammler, G. Beaucage, R. Mueller, and S. E. Pratsinis, Langmuir **20**, 1915 (2004).

[30] z can also be estimated from the radii of gyration from the two levels of structure [28],

$$z_{R_g} \sim \left(\frac{R_{g,2}}{R_{g,1}} \right)^{d_f}, \qquad (4')$$

under the assumption that R_g is a direct measure of size both for the primary particles and for the aggregates. This assumption is paramount to an assumption of a narrow distribution in both aggregate and primary particle size. Equation $(4')$ reflects a higher-order moment than Eq. (4)—i.e., a larger value with potentially weaker agreement with other techniques. A power-series expansion of Eq. (1), $I(q) = N r_e^2 \rho^2 V^2 (1 - q^2 R_g^2 / 3 + \cdots)$, for small $q R_g$, shows that $\langle R_{g,2}^2 \rangle$ is proportional to $\langle z^{2+(2/d_f)} \rangle / \langle z^2 \rangle$, since $\rho^2 V^2 \sim z^2$ and $R_{g,2}^2 \sim z^{2/d_f}$. (r_e is the classical electron radius, ρ is the electron density of the particles, and V is the particle volume.) Then,

$$\left(\frac{R_{g,2}^2}{R_{g,1}^2}\right)^{d_f/2} = \left(\frac{\langle z^{2+(2/d_f)}\rangle}{\langle z^2\rangle}\right)^{d_f/2} = z_{R_g}, \qquad (4'')$$

assuming monodisperse primary particles. For $d_f=2$,

$$\left(\frac{R_{g,2}^2}{R_{g,1}^2}\right) = \frac{\langle z^3\rangle}{\langle z^2\rangle},$$

for instance. Additionally, functions that involve integrals of the scattered intensity can also yield moments of z.

[31] P. J. Flory, *Principles of Polymer Chemistry* (Cornell University Press, Ithaca, NY, 1978).

[32] W. R. Krigbaum and P. J. Flory, J. Am. Chem. Soc. **75**, 1775 (1953).

[33] J. des Cloizeaux, Phys. Rev. A **10**, 1665 (1974); J. des Cloizeaux and G. Jannink, *Polymers in Solution: Their Modelling and Structure* (Clarendon, Oxford, 1990).

[34] H. Benoit, C. R. Hebd. Seances Acad. Sci. **245**, 2244 (1957).

[35] P. Meakin, Prog. Solid State Chem. **20**, 135 (1990).

[36] P. Meakin, I. Majid, S. Havlin, and H. E. Stanley, J. Phys. A **17**, L975 (1984).

[37] S. I. Yun, R. M. Briber, R. A. Kee, and M. Gauthier, Polymer **44**, 6579 (2003).

[38] P. Debye, J. Phys. Colloid Chem. **51**, 18 (1947); R. M. Fuoss, *The Collected Papers of Peter J. W. Debye* (Interscience, New York, 1954).

[39] R. Thouy and R. J. Jullien, J. Phys. I **6**, 1365 (1996).

[40] A. Peterlin, Makromol. Chem. **9**, 244 (1953).

[41] M. Antonietti and C. Rosenauer, Macromolecules **24**, 3434 (1991).

[42] M. Lattuada, H. Wu, and M. Morbidelli, J. Colloid Interface Sci. **268**, 106 (2003).

[43] A. Hasmy and R. Jullien, J. Non-Cryst. Solids **186**, 342 (1995).

[44] M. Carpineti, F. Ferri, M. Giglio, E. Paganini, and U. Perini, Phys. Rev. A **42**, 7347 (1990).